

Article

# Comparison of the Microstructure Evolution and Wear Resistance of Ti6Al4V Composite Coatings Reinforced by Hard Pure or Ni-Plated Cubic Boron Nitride Particles Prepared with Laser Cladding on a Ti6Al4V Substrate

Shuren Fu <sup>1,2</sup>, Lijing Yang <sup>1,\*</sup>, Pei Wang <sup>1</sup>, Shaopeng Wang <sup>1</sup> and Zhengxian Li <sup>1,2</sup>

<sup>1</sup> Northwest Institute for Non-Ferrous Metal Research, Xi'an 710016, China; fushuren07@126.com (S.F.); nwpupw@126.com (P.W.); ffs1@c-nin.com (S.W.); lzxqy725@163.com (Z.L.)

<sup>2</sup> School of Material Science and Engineering, Northeastern University, Shenyang 110819, China

\* Correspondence: yanglj@c-nin.com

Received: 18 June 2020; Accepted: 16 July 2020; Published: 20 July 2020



**Abstract:** Titanium alloy is a major structural material with excellent high specific strength in aerospace applications. Cubic boron nitride (cBN) is a synthetic wear-resistant material with high hardness, similar to that of diamond, that is used in mechanical cutting and grinding. In addition, the thermal stability of cubic boron nitride particles is much better than that of diamond. In order to further enhance the wear resistance of the Ti6Al4V alloy, the laser cladding (LC) technology characteristics of metallurgical bonding were used to prepare cubic boron nitride/Ti6Al4V and Ni-plated cubic boron nitride/Ti6Al4V composite coatings on Ti6Al4V substrates in this paper. However, in the laser molten pool, it is difficult to retain the raw properties of cubic boron nitride particles under laser radiation. Both composite coatings were analyzed using scanning electron microscopy (SEM), energy dispersive spectroscopy (EDS), X-ray diffraction (XRD), and X-ray photoelectron spectroscopy (XPS). The microstructures and interface bonding between cubic boron nitride particles and the Ti6Al4V matrix were examined using SEM, and the wear resistance and the worn track morphology of the composite coatings were evaluated using the ball-on-disc wear test and step profiler (WTM-2E). The results indicated that the Ni-plated cubic boron nitride/Ti6Al4V composite coating showed fewer thermal defects in comparison with the cubic boron nitride/Ti6Al4V coating. The Ni plating on the surface of cubic boron nitride particles was able to avoid the generation of thermal cracking of the cubic boron nitride particles in the composite coating. The TiN reaction layer was formed between the cubic boron nitride particles and Ti6Al4V matrix, which effectively prevented the further decomposition of the cubic boron nitride particles. The XRD and XPS results confirmed that the TiN reaction layer formed between the cubic boron nitride particles and Ti6Al4V. The Ni plating on the surface of the cubic boron nitride particles was also beneficial for increasing the wear resistance of the composite coating.

**Keywords:** laser cladding; cubic boron nitride particle; Ti6Al4V alloy; composite coating; wear

## 1. Introduction

Titanium alloy is an aerospace structural material with excellent high specific strength [1]. In the process of the high-speed rotation of titanium alloy compressor blades of aero-engines, the blade tip is prone to failure due to scraping between the Al-Si polymer sealing coating of the engine casing and the titanium alloy blade tip [2]. In order to enhance the wear resistance of the blade tip and maintain a

reasonable gap between the blade tip and the engine casing, preparation technology for the surface coating is used to improve the wear resistance of the titanium alloy blade tip. At present, the coating preparation technologies that can be used to improve the wear resistance of titanium alloy materials mainly include thermal spraying, cold spraying, physical vapor deposition (PVD), micro-arc oxidation (MAO), laser cladding, electroplating, etc.

However, the bonding mechanisms of thermal spraying and cold spraying coatings with a metal substrate are primarily mechanical interlockings, which are prone to cause coat peeling under high temperatures and heavy loads due to the poor adhesion [3,4]. The coating prepared by PVD, which has excellent adhesion, is only a submicron-thin film [5]. Numerous pores will be formed in the coating owing to the discharge during the process of MAO [6]. The serious environmental pollution from the electroplating technology limits its further application [7]. The laser cladding (LC) technology characteristic of metallurgical melting not only improves the surface performance of related materials but also guarantees the bonding strength between the coating and substrate, therefore, LC is suitable for preparing a hard particle reinforced wear-resistant coating [8].

Metal matrix composites can be easily prepared on titanium alloy surfaces using LC. There are primarily two types of metal matrix composite coatings, which include ceramic particles directly added into metal matrix materials and ceramic particles formed by an in-situ reaction during the laser cladding process [9]. For various engineering applications, the former is produced by the introduction of ceramic feedstocks, including carbide, nitride, boride, and oxide ceramic, into the laser molten pool. The latter is prepared by an in-situ reaction to form hard phases, such as TiC, TiN, TiB, WC, Al<sub>2</sub>O<sub>3</sub>, and other reinforced phases in the laser-generated melt pool [9]. However, the hard particles of the composite coating require excellent machinability and abrasion resistance during the scraping process between the blade tip and casing sealing coating.

One hard synthetic material is cubic boron nitride (cBN) with a high hardness for mechanical cutting and grinding, similar to that of diamond. The thermal stability of cBN particles is much better than that of diamond [10]. In the atmosphere, diamond will be prone to generate a graphitization phase transition as soon as the temperature reaches 600 °C, while cBN particles do not undergo phase transition until 1300 °C [11–13]. Therefore, cBN is suitable for preparing a wear-resistant composite coating on a titanium alloy blade tip using LC, owing to its outstanding machinability and thermal stability [14].

At present, the preparation of boron nitride reinforced composite coatings by LC is rarely studied. In industrial applications, boron nitride is typically divided into cubic boron nitride (cBN) and hexagonal boron nitride (hBN) [14]. The majority of research with respect to hBN is focused on self-lubricating coatings. Lu et al. investigated the Ni60/h-BN self-lubricating coating prepared by laser cladding technology on 0Cr18Ni9 stainless steel substrates [15]. However, the preparation of cBN reinforced composite coatings using laser cladding is rarely researched. Gupta et al. [16] prepared boron carbide and cubic boron nitride reinforced Ti6Al4V matrix composites using continuous wave SPI fiber laser direct metal laser-sintering (DMLS) technology, and the results indicated that the Ti6Al4V-B<sub>4</sub>C-cBN metal matrix composites showed good affinity with each other. This technology can also be used to prepare various intermetallic composite coatings.

Pacella et al. [17] suggested that allotropic transformations of cBN into amorphous boron nitride and hBN were identified below the ablated surface and down to depths exceeding 300 nm in high laser thermal radiation. Thepsonthi et al. [13] investigated the performance of cBN coated and uncoated micro-end mills in terms of the surface roughness, burr formation, and tool wear, aiming to improve the performance of carbide micro-end mills by applying a cBN coating. Yedave et al. [18] investigated the synthesis and performance of a novel cBN-TiN composite coating, which was prepared in a two-step process, including an electrostatic spray coating of cBN particles and chemical vapor infiltration of TiN.

While the chemical and thermal stability of cBN particles are much better than that of diamond, it is difficult for cBN particles to maintain their original properties without phase transition and decomposition. In this paper, cBN/Ti6Al4V and Ni<sub>60</sub>cBN/Ti6Al4V composite coatings were

prepared by LC on a Ti6Al4V alloy substrate. The microstructure, phase composition, cBN particle evolution, and interface evolution between cBN and the Ti6Al4V matrix of the cBN/Ti6Al4V and NicBN/Ti6Al4V composite coatings were investigated, and the abrasion resistance of the composite coatings was evaluated.

## 2. Materials and Methods

### 2.1. Experimental Material

Specimens with dimensions of  $100 \times 50 \times 10 \text{ mm}^3$  were machined from a Ti6Al4V substrate. The oxide layer was removed before laser cladding and the grease was cleaned with acetone. As shown in Figure 1a, commercially available Ti6Al4V alloy powder (Sino-Euro Materials Technologies of Xi'an Co., Ltd., Xi'an, China), with particle sizes ranging from 10 to 45  $\mu\text{m}$ , was prepared by high-speed rotating atomization. As shown in Figure 1b,c, the commercially available cubic boron nitride (cBN) powder and nickel-plated cBN powder (NicBN) (Mingshan New Materials Technologies of Nanjing Co., Ltd., Nanjing, China), with particle sizes ranging from 20 to 35  $\mu\text{m}$ , were produced using the high temperature and high pressure method. The NicBN powder with 60% increasing particle weight was produced by chemical Ni-plating. Figure 1d is the cross-section view of NicBN. As demonstrated in Figure 1, the cBN and NicBN powder showed irregular shapes and the Ni-plating thickness of the NicBN particle was approximately 2–5  $\mu\text{m}$ . As shown in Table 1, the surface elements of Ti6Al4V, cBN, and NicBN particles were analyzed with energy dispersive spectroscopy (EDS). The results showed that the contents of the B and N elements on the surface of the cBN particles were 45.57 and 54.43 wt.%, and the contents of the P and Ni elements on the surface of the NicBN particles were 7.97 and 92.03 wt.%, respectively.

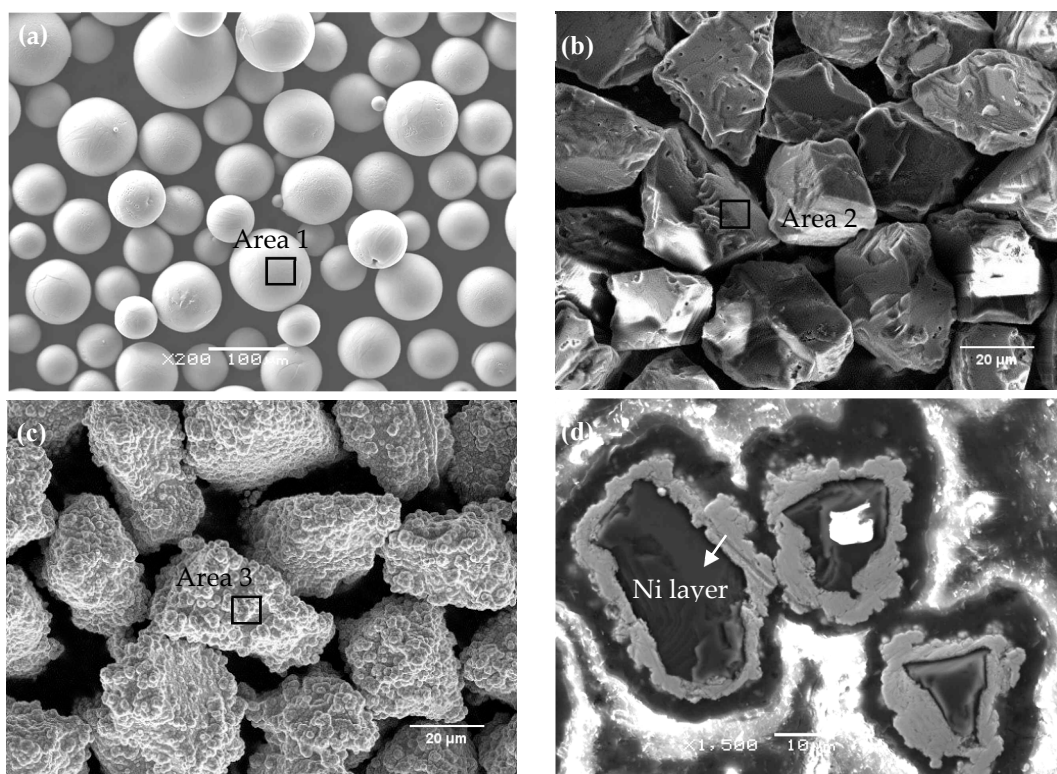


**Figure 1.** Morphologies of the Ti6Al4V, cubic boron nitride (cBN) powder and nickel-plated cBN powder (NicBN): (a) Ti6Al4V particles; (b) cBN particles; (c) NicBN particles; and (d) Ni coating.

**Table 1.** The elemental concentration of the selected areas in Figure 1.

Element (wt.%)	Ti	Al	V	C	B	N	Ni	P
Area 1	92.52	3.93	2.82	0.74	–	–	–	–
Area 2	–	–	–	–	45.57	54.43	–	–
Area 3	–	–	–	–	–	–	92.03	7.97

## 2.2. Preparation of Composite Coating

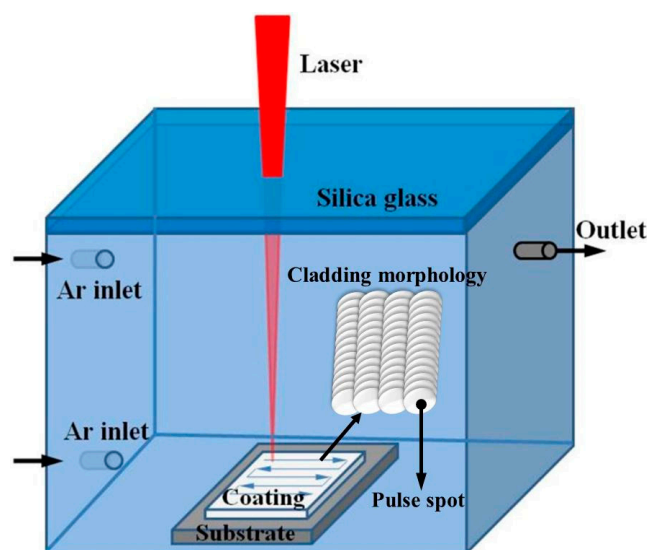
The pulsed Nd: YAG laser system (JHM-1GY-400D) was used to prepare the cBN/Ti6Al4V and NicBN-Ti6Al4V composite coatings in this study. The effective energy ( $E_{con}$ ) was used as an indicator to examine the effects of the processing parameters on the cladding quality and formability [19]. In the continuous laser cladding process, this energy was responsible for heating/melting the substrate surface and powder stream and was calculated through Equation (1) [19]. In the pulse laser cladding process, the effective energy can be expressed by Equation (2).

$$E = \frac{P}{V \times D} \quad (1)$$

$$E_{pul} = \frac{P \times W}{D} \quad (2)$$

Here,  $P$  is the laser power (W),  $V$  is the scanning speed (mm/s),  $w$  is the pulse width (ms), and  $D$  is the laser spot size (mm). The pulse laser cladding track is composed of a large number of pulse cladding spots. The laser duration at each cladding spot is the pulse width, which is effective to reduce the immersed time for the cBN particles in the molten pool.

The particle volume ratios of cBN or NicBN vs. Ti6Al4V for producing the composite coatings raw material were the same (30 vol.% cBN + 70 vol.% Ti6Al4V and 30 vol.% NicBN + 70 vol.% Ti6Al4V). Both the cBN/Ti6Al4V and NicBN/Ti6Al4V composite coatings were prepared using the same process parameters. During the LC process, the parameters were 5 ms of pulse width, 150 A of current, 18 Hz of pulse frequency, 4 mm/s scanning speed, and 40% lap rate. The LC experiment was performed in a closed protective box filled with Ar gas. The box was made of high-temperature silica glass with a thickness of 3 mm. The laser beam passed through the silica glass to melt the composite powder. The schematic diagram is shown in Figure 2. Before the experiment, Ti6Al4V alloy powder was dried at 110 °C in a vacuum oven for 60 min.

**Figure 2.** Schematic diagram of the protective box in the laser cladding (LC).

### 2.3. Characterization Methods

The cross-sectional coating specimens were cut by wire electrical discharge machining. The coating specimens were ground and polished like a mirror, and then etched for 10 s with a corrosive solution of 1 mL HF: 4 mL HNO<sub>3</sub>: 45 mL H<sub>2</sub>O. The composite coating specimens were examined using scanning electron microscopy (SEM, JSM-6460, JEOL, Tokyo, Japan) and X-ray diffraction (XRD, D8 Advance, Bruker, Germany) to analyze the microstructure of the composite coating, the distribution of cBN particles, and the phase composition. We investigated the composite coating and worn surface using energy dispersive spectroscopy (EDS, NanoXflash Detector 5010, Bruker, Germany). We used X-ray photoelectron spectroscopy (XPS, ESCALAB 250Xi, Thermo Fisher Scientific, Waltham, MA, USA) to distinguish the binding energy of chemical elements. The XPS analysis was operated at 100.0 and 30.0 eV to generate monochromatic Al K alpha radiation; the spot sizes of the radiation were 500 and 650 μm; the energy step sizes were 1.0 and 0.1 eV.

The wear resistance of the composite coating was tested and the worn track morphology was evaluated using the ball-on-disc wear test and step profiler (WTM-2E) at room temperature, respectively. The pin was a Si<sub>3</sub>N<sub>4</sub> ceramic ball with a 4 mm diameter. The disk was tested composite coatings. The test was performed under a load of 4.9 N at a rotational speed of 1000 rpm. The sliding time duration was 120 min and the radius of the wear track was 3 mm.

## 3. Results

### 3.1. Microstructure of Composite Coatings

Two kinds of composite coatings with powder ratios of 30 vol.% cBN + 70 vol.% Ti6Al4V and 30 vol.% NicBN + 70 vol.% Ti6Al4V were deposited onto a Ti6Al4V substrate under the same parameters by LC. The comparison of the cross-sectional microstructure of the cBN/Ti6Al4V and NicBN/Ti6Al4V composite coatings is shown in Figure 3. The discontinuous heating characteristic of a pulse laser can reduce the substrate dilution. We observed that the forming thickness and cross-sectional morphology of the NicBN/Ti6Al4V composite coating were more uniform and denser than the cBN/Ti6Al4V composite coating, see Figure 3a,b. As demonstrated in Figure 3c,d, the bonding between the coatings and substrate was mainly metallurgical bonding and the hard cBN particles were evenly embedded in the coatings. Despite that the content of the cBN particles retained in the cBN/Ti6Al4V coating was significantly higher than that of the NicBN/Ti6Al4V, some pores and lamellar cracking between the coating and the substrate were observed in the cBN/Ti6Al4V coating.

Figure 3e,f are backscattered electron images (BSE) of the microstructure of the two composite coatings, the black zones of Figure 3e,f are cBN particles, which were used to calculate the content of the cBN particles of the composite coatings. According to the calculation of the black cBN particle area using Image-Pro Plus software, the volume ratios of the cBN particles in Figure 3e,f were 44.2 and 24.3 vol.%, respectively. The 19.9% difference of volume percentage of cBN particles in these two composite coatings was due to the Ni plating, which prevented further melting of cBN into the Ti6Al4V matrix.

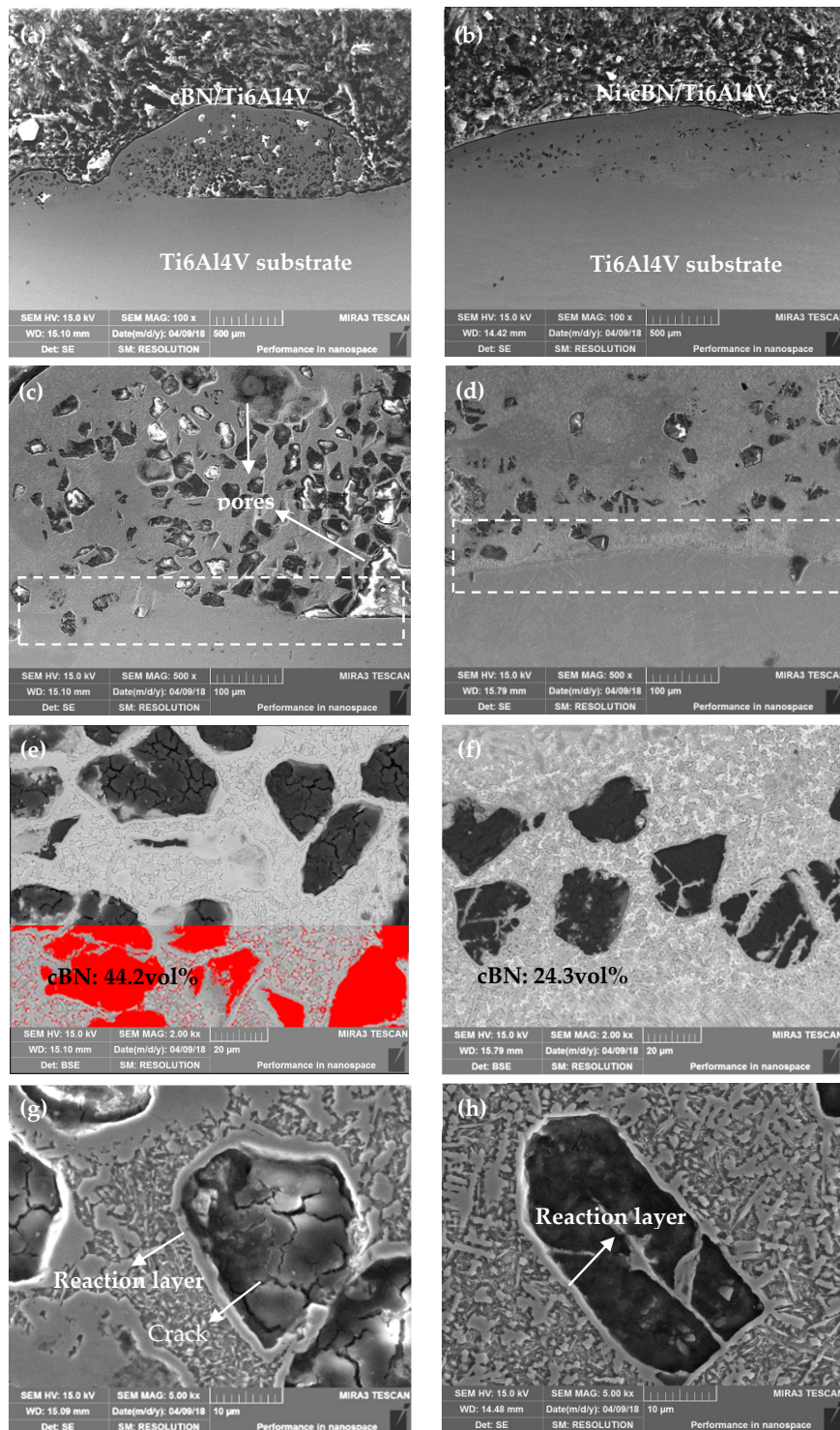


**Figure 3.** Cross-sectional SEM images of the LC cBN/Ti6Al4V and Ni-cBN/Ti6Al4V composite coatings: (a) Macroscopic image of the cBN/Ti6Al4V coating; (b) macroscopic image of the Ni-cBN/Ti6Al4V coating; (c) interface of the cBN/Ti6Al4V coating; (d) interface of the Ni-cBN/Ti6Al4V coating; (e) backscattered electron (BSE) image of the cBN/Ti6Al4V coating; (f) BSE image of the Ni-cBN/Ti6Al4V coating; (g) cBN particles in the cBN/Ti6Al4V coating; and (h) cBN particles in the Ni-cBN/Ti6Al4V coating.

The SEM images at high magnification of the cBN particles of the LC microstructures are shown in Figure 3g,h. The cBN particles in both composite coatings were coated with a 2–5  $\mu\text{m}$  reaction layer at the interface between the cBN particles and the Ti6Al4V matrix. In addition, more cracks were

present on the surface of cBN particles in the cBN/Ti6Al4V coating. This suggests that the Ni plating on the surface of cBN particles improved the quality of the composite coating, reduced the generation of cladding defects, and prevented the cBN particles from cracking in the laser molten pool.

### 3.2. Interface Reaction of cBN Particles

According to the comparison of the microstructure of the cBN/Ti6Al4V and NicBN/Ti6Al4V composite coatings in Figure 3, the submicron reaction layers formed at the interface between the cBN particles and Ti6Al4V matrix regardless of whether the cBN particles were coated with nickel. The EDS mapping of the interface between the coating and substrate is shown in Figure 4. The Ti element from the Ti6Al4V matrix did not diffuse into the cBN particle. We further analyzed the distribution of elements around the cBN.

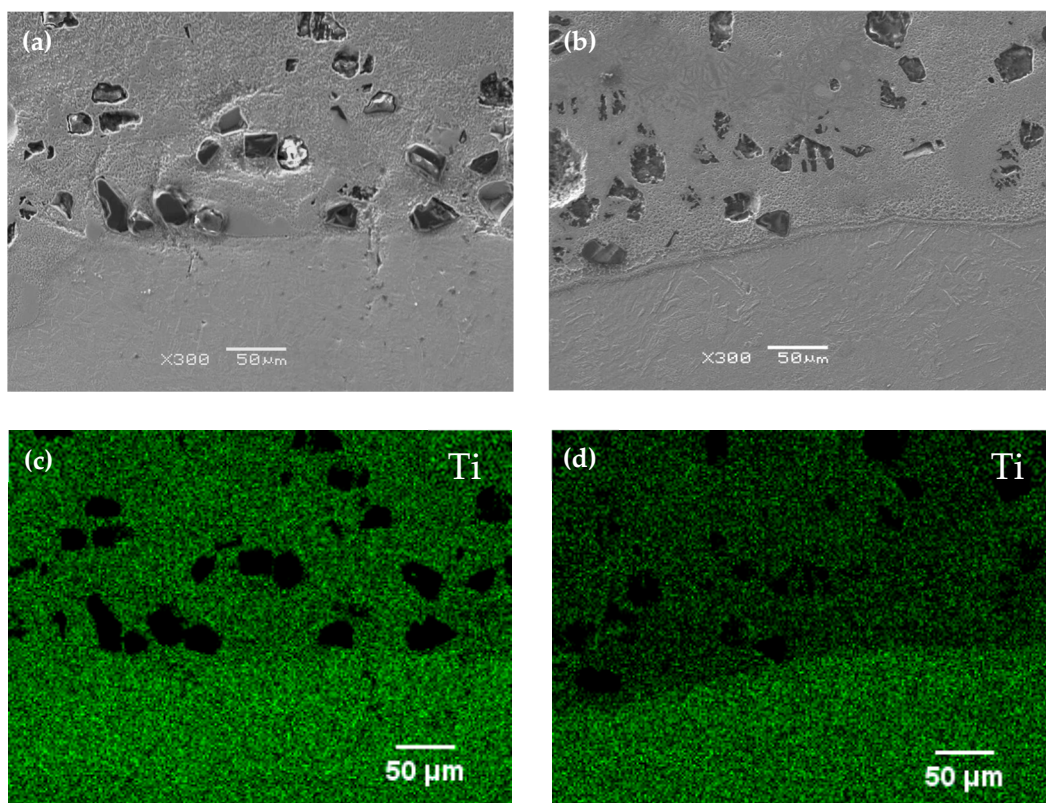


**Figure 4.** SEM and energy dispersive spectroscopy (EDS) mapping of interface between the coating and substrate: (a) cBN/Ti6Al4V coating; (b) NicBN/Ti6Al4V coating; (c) Ti element mapping of (a); and (d) Ti element mapping of (b).

The cBN particle image in Figure 3g was obtained with EDS mapping and the results of the elemental distribution are shown in Figure 5b. We found that the EDS scanning signals of the Ti and N elements at the interface reaction layer were strong, which indicates that the Ti element from the Ti6Al4V matrix did not diffuse into the cBN particle but concentrated in the reaction layer, and the content of the N element was higher at the interface.

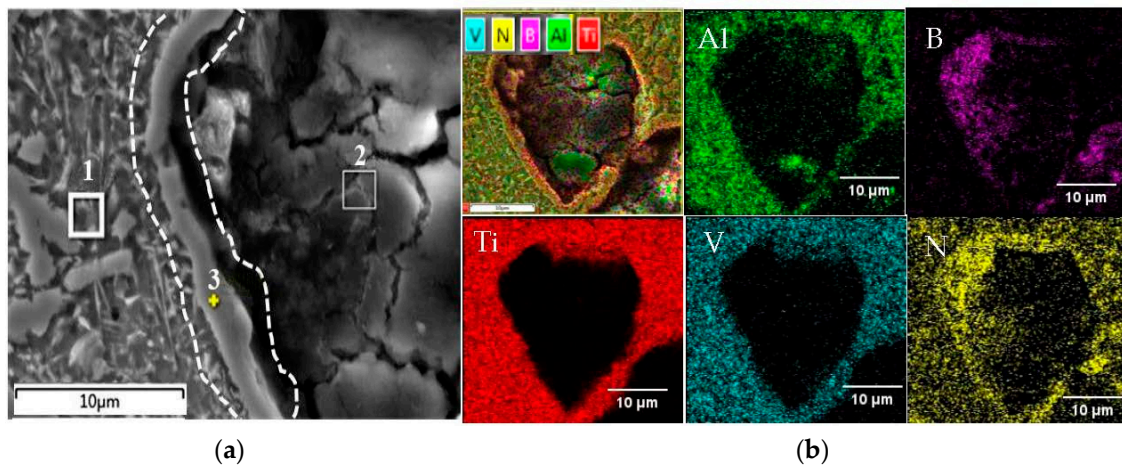


**Figure 5.** Images of SEM and EDS: (a) SEM image at the interface of a cBN particle; (b) element mapping of a cBN particle in the composite coating.

From Figure 5a, the Ti6Al4V matrix (area 1), interface (area 2), and cBN particle (area 3) were detected by means of the EDS analysis. The results of the elemental content at these three regions are reported in Table 2. The results show that the elements of areas 1 and 2 were essentially consistent with the original Ti6Al4V and cBN particles, respectively. However, the elements of area 3 at the reaction layer consisted of 79.23 wt.% Ti and 20.77 wt.% N elements, which indicate that the Ti element from the Ti6Al4V alloy and N element from cBN were prone to react and form a  $Ti_xN_y$  transition layer at the interface.

**Table 2.** Elemental concentration of the selected areas of the cBN/Ti6Al4V interface.

Elements(wt.%)	B	N	Ti	Al	V
Area 1	–	–	89.77	7.27	2.96
Area 2	43.35	56.65	–	–	–
Area 3	–	20.77	79.23	–	–

### 3.3. Phases of the NicBN/Ti6Al4V Composite Coating

Combined with the microstructure and EDS analysis of the composite coating, NicBN particles were also prone to react with the Ti6Al4V matrix to form a submicron  $Ti_xN_y$  reaction layer. XRD analysis was applied on the NicBN/Ti6Al4V powder and LC composite coating as shown in Figure 6a,b, respectively. The diffraction result of the NicBN/Ti6Al4V composite powder was a Ti solid solution, with cBN,  $Ni_2P$ , and  $NiP_2$ . Both the  $Ni_2P$  and  $NiP_2$  phases originated from the electroless nickel plating process. The phases of the NicBN/Ti6Al4V composite coating were composed of Ti solid solution,  $Ni_3P$ , TiN,  $TiB_x$ , and BN. According to the EDS and XRD results of the NicBN/Ti6Al4V composite coating, the cBN particles were partially decomposed into TiN and  $TiB_x$  at the region between Ti6Al4V and cBN during the laser cladding process.

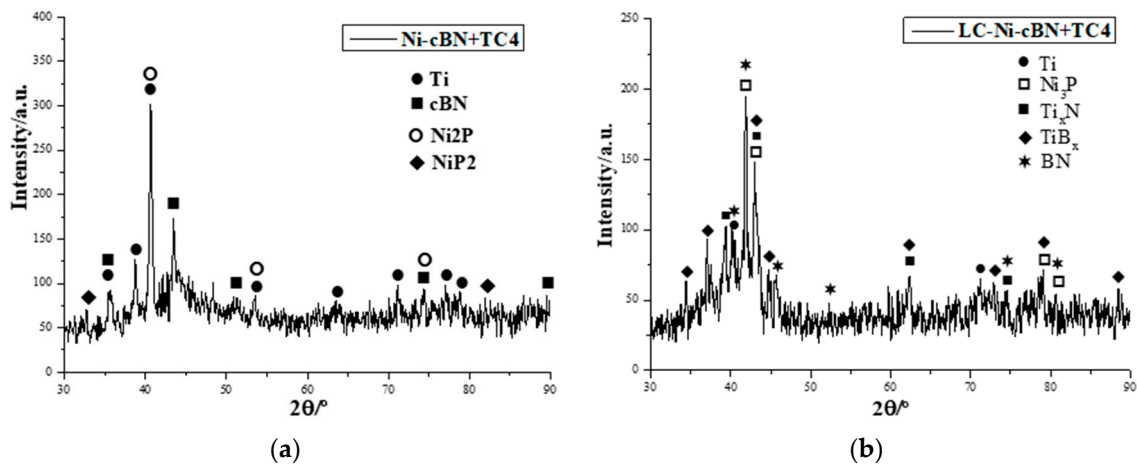


**Figure 6.** XRD patterns: (a) NicBN/Ti6Al4V composite powder; and (b) NicBN/Ti6Al4V composite coating.

### 3.4. XPS Analysis of the NicBN/Ti6Al4V Composite Coating

In order to further confirm the new phase in the NicBN/Ti6Al4V composite coating, the binding energy of B and N from the cBN powder and NicBN/Ti6Al4V composite coating were detected using XPS, which can be used to identify the compounds formed by the B and N elements. After the specimens were etched with argon ions for 60 s, the full-spectrum scanning and high resolution spectral analysis results of B and N of the cBN powder and composite coating were determined as demonstrated in Figure 7.

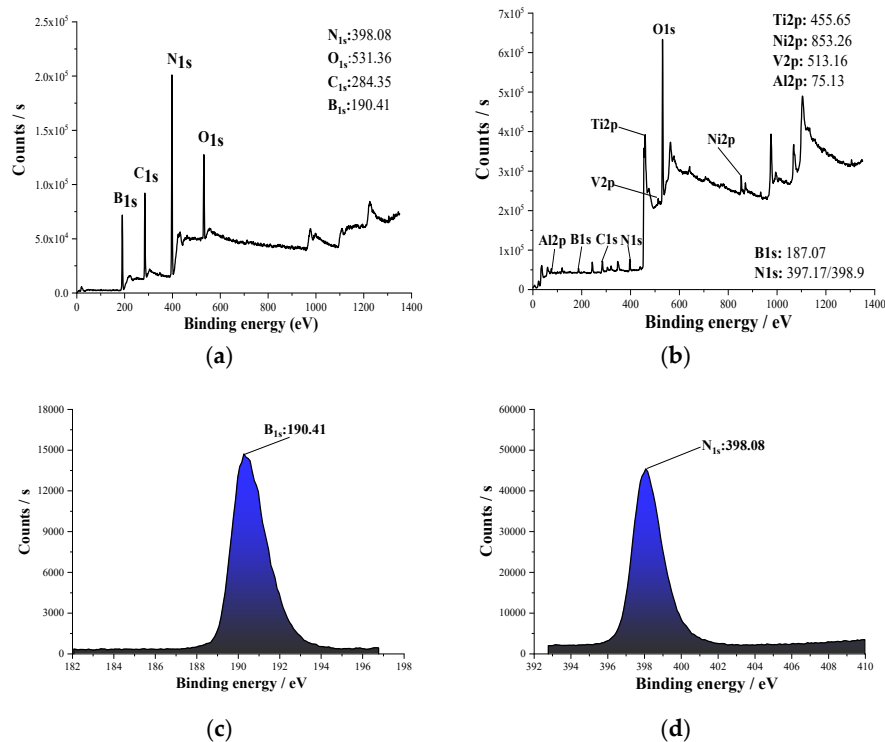


**Figure 7.** Cont.

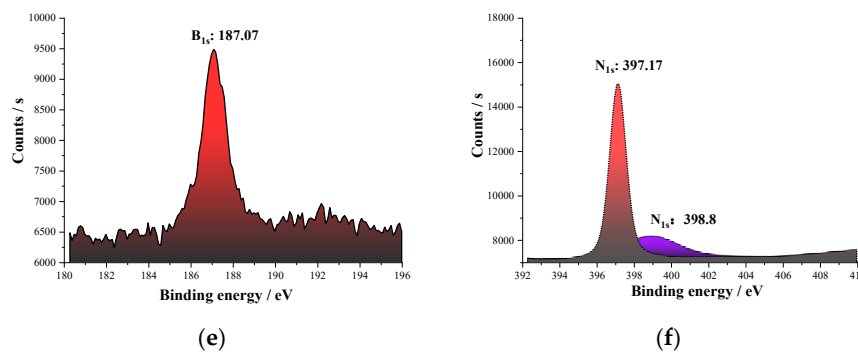


**Figure 7.** X-ray photoelectron spectroscopy (XPS) patterns: (a,b) Survey spectra scanning of the cBN powder and NicBN/Ti6Al4V composite coating; (c,e) high resolution spectral analysis of the B1s peak of the cBN powder and NicBN/Ti6Al4V composite coating; (d,f) high resolution spectral analysis of the N1s peak of the cBN powder and NicBN/Ti6Al4V composite coating.

In the cBN powder, as shown in Figure 7c,d, the binding energy of the B and N elements were 190.41 and 398.08 eV, respectively. However, in the NicBN/Ti6Al4V composite coating, the binding energy of B decreased to 187.07 eV and the binding energies of N changed to 397.13 and 398.8 eV, as shown in Figure 7e,f. We observed that the satellite peak appeared in the N1s high resolution spectrum of the composite coating as shown in Figure 7f. Referring to the handbook of X-ray photoelectron spectroscopy and the standard binding energy of N and B elements in the original cBN particle, the TiB phase was formed when the binding energy of B was 187.07 eV, the TiN phase was formed when the binding energy of N was 397.13 eV, and the BN phase was formed when the binding energy of N was 398.8 eV. The binding energy of B and N in the LC NicBN/Ti6Al4V composite coating indicated that the TiN and TiB phases were generated due to part of the cBN particle transformation and decomposition.

### 3.5. Hardness of Coatings

The hardness variation curves for the composite coatings obtained under an indentation load of 4.903 N (HV0.5) are presented in Figure 8. The average hardness of the NicBN/Ti6Al4V composite coating was  $624.89 \pm 191.64$  HV and that of cBN/Ti6Al4V was  $617.9 \pm 169.87$  HV. The hardness values of these two composite coatings are close. For both composite coatings, the hardness of the coating is much higher than that of the substrate, which is attributed to the reinforcement of hard cBN particles.

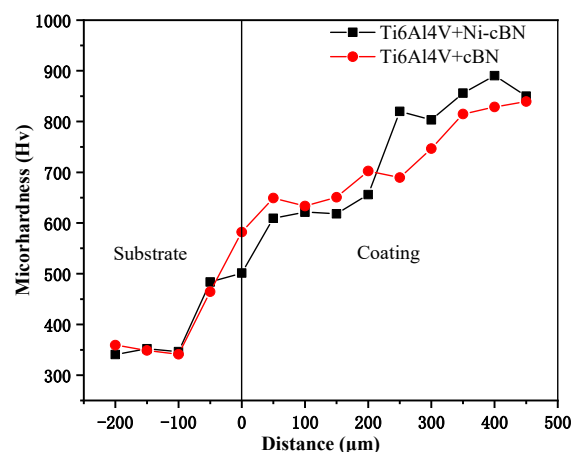


**Figure 8.** The microhardness of the NicBN/Ti6Al4V and cBN/Ti6Al4V composite coatings.

### 3.6. Wear Resistance

Under an atmospheric environment and dry-sliding wear, the wear resistances of the cBN/Ti6Al4V and NicBN/Ti6Al4V composite coatings were tested using the ball-on-disc mode at room temperature.

The curve of the friction coefficient, along with the sliding time, was recorded and is shown in Figure 9. According to the friction coefficient curve, the variations of the friction coefficient of the Ni-cBN/Ti6Al4V composite coating were more stable than those of the cBN/Ti6Al4V composite coating. As for the cBN/Ti6Al4V composite coating, the friction coefficient significantly fluctuated between 0.3623 and 0.2671 with a sliding time range from 10 to 60 min, and then the friction coefficient gradually dropped to a lower value and became more stable. The average friction coefficients of the cBN/Ti6Al4V and Ni-cBN/Ti6Al4V composite coatings were 0.3196 and 0.2691, respectively. The more stable curve and lower friction coefficient that we detected in the Ni-cBN/Ti6Al4V composite coating were due to the good cutting action of the irregular cBN particles, which were retained in the composite coating without cracking during the LC process.

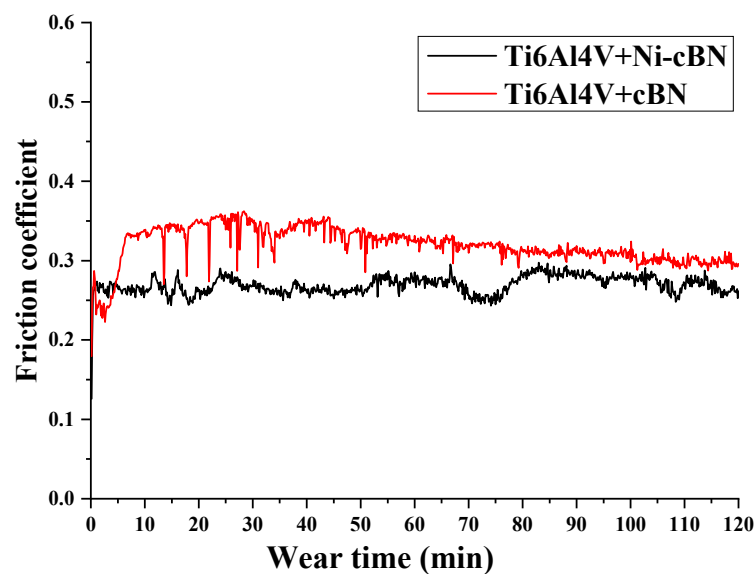
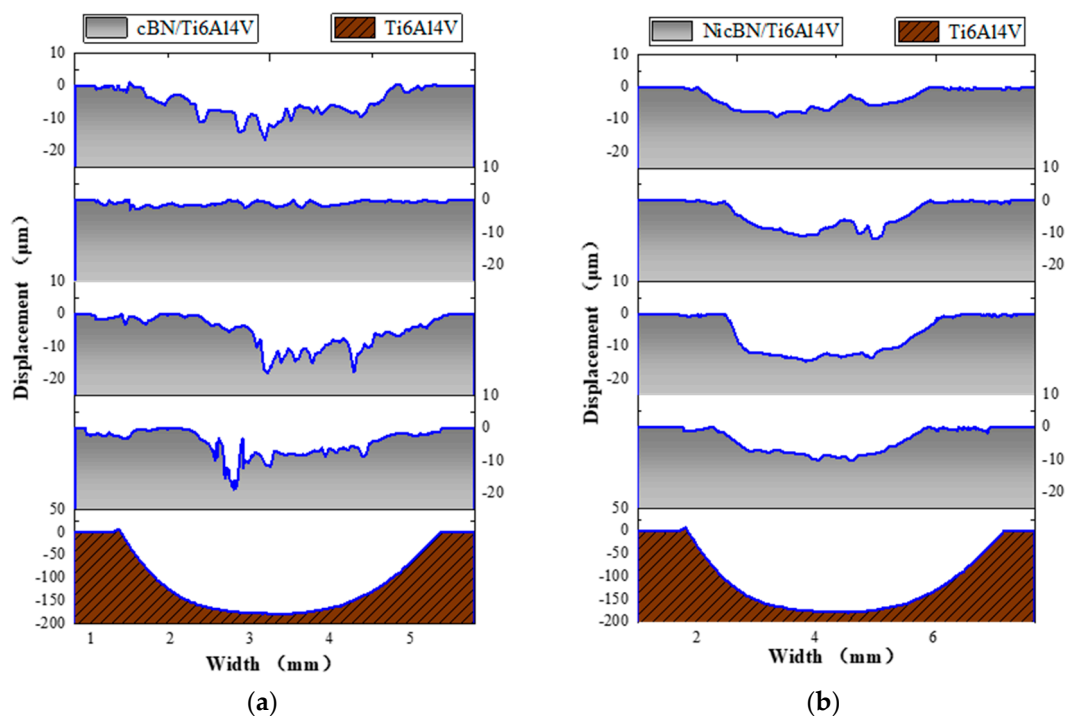


Figure 9. Variations of the friction coefficient with a sliding time range.

In order to further evaluate the abrasion loss, the cross-sectional profile curves of a worn track were operated at four different locations of circular grinding track using the step profiler scribe, which moved uniformly along a straight line at a load of 0.05 N. The displacement curves of the scribe are exhibited in Figure 10. From Figure 10a, the profile curve of the worn track of the cBN/Ti6Al4V composite coating irregularly fluctuated; thus, we were unable to accurately obtain the abrasive track width and area. However, the maximum abrasive depth of the cBN/Ti6Al4V composite coating was 18  $\mu\text{m}$ .



**Figure 10.** The profile curves of the worn cross-section: (a) The cBN/Ti6Al4V composite coating; (b) the NicBN/Ti6Al4V composite coating.

The irregular profile curve is attributed to the crushing and shedding of cBN particles in the cBN/Ti6Al4V composite coating under the scraping and grinding of the  $\text{Si}_3\text{N}_4$  pin. The profile curve of the worn NicBN/Ti6Al4V composite coating was clear and regular, as shown in Figure 10b. The mean worn width and maximum depth were in the range of 9.56–14.29  $\mu\text{m}$  and 1.1–1.4 mm at the four positions of the worn track. The cross-sectional area of the worn track was obtained by integrating the profile curves using Origin software. The mean value of the cross-sectional worn area was  $19.20 \pm 1.24 \mu\text{m}^2$ .

The volume loss was estimated by calculating the volume of the wear track (worn scratch), which is the area of the cross profile multiplied by the periphery of the wear track. The wear loss was 361.73  $\mu\text{m}^3$ . Compared with the cBN/Ti6Al4V composite coating, the regular profile curve of the worn track of the NicBN/Ti6Al4V composite coating indicated that only a small part of the cBN particles were crushed in the grinding process. In addition, as shown in Figure 10, both the cBN/Ti6Al4V composite coating and NicBN/Ti6Al4V composite coating demonstrated much better wear resistance than the Ti6Al4V substrate.

In order to further understand the wear test results, the worn tracks of the cBN/Ti6Al4V and NicBN/Ti6Al4V composite coatings were observed using SEM, as shown in Figure 11. We observed that the cBN particles in the cBN/Ti6Al4V composite coating were prone to crack and spall off, while the Ni-coated cBN particles in the NicBN/Ti6Al4V composite coating remained unbroken, as demonstrated in Figure 11a,b,e,f. In addition, as indicated in Figure 11a,b, the worn surface areas of the  $\text{Si}_3\text{N}_4$  balls were different. Area 1 was  $1.93 \times 10^6 \mu\text{m}^2$  and area 2 was  $1.55 \times 10^6 \mu\text{m}^2$ , which indicates that the scraping and grinding degrees of these two composite coatings were clearly different.

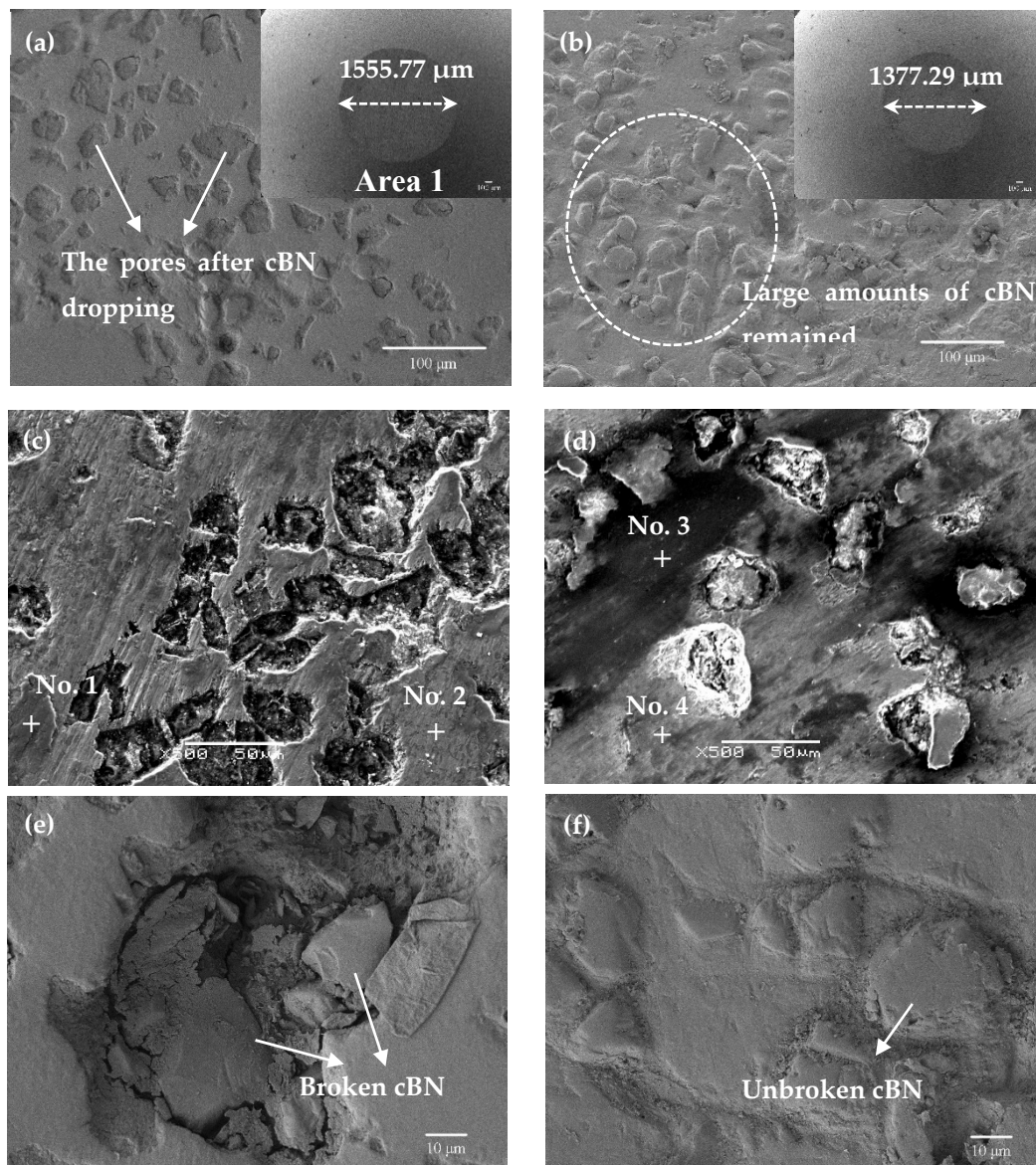


**Figure 11.** SEM images of the worn surface: (a,c,e) cBN/Ti6Al4V composite coating; (b,d,f) NicBN/Ti6Al4V composite coating.

As shown in Figure 11c,d, the worn surfaces of both composite coatings displayed noticeable black adhesive. The EDS analysis results of different areas in Figure 11c,d are demonstrated in Table 3. The oxygen contents of No. 1 and No. 3 reached 38.47 and 42.28 wt.%, which indicates that the Ti6Al4V alloy matrix oxidized during the grinding process. The Si contents of No. 1 and No. 3 were 13.56 and 17.15 wt.%, which stems from the scraping of cBN particles against the Si<sub>3</sub>N<sub>4</sub> ball during the dry friction process.

**Table 3.** Elemental concentrations (wt.%) of the selected areas of the worn surface using EDS.

Elements(wt.%)	O	C	Ti	Al	V	Ni	Si
No. 1	38.47	–	40.34	4.86	2.77	–	13.56
No. 2	19.56	–	66.83	6.59	4.47	–	2.55
No. 3	42.28	4.78	21.60	2.30	–	11.88	17.15
No. 4	17.38	5.37	62.34	2.07	3.08	5.85	3.90

The higher contents of Si and O in No. 3 suggest that the NicBN/Ti6Al4V composite coating had better cutting and grinding ability. The Ni elements of No. 3 and No. 4 likely arise from the Ni plating of NicBN particles. The above EDS results demonstrated that the Ti6Al4V alloy matrix bonded with cBN particles was prone to oxidize in the dry wear process. On the basis of the worn tracks, we found that the Ni coated on the surface of cBN particles significantly prevented the thermal damage of cBN particles in the laser molten pool and improved the wear resistance of the NicBN/Ti6Al4V composite coating.

#### 4. Discussion

According to the microstructure of the cBN/Ti6Al4V and NicBN/Ti6Al4V composite coatings, Ni plating of cBN particles were beneficial for improving the quality of composite coatings and prevent thermal cracking defects in cBN particles in the laser molten pool. In addition, Ni plating of cBN particles avoided direct contact between the laser high-energy beam and cBN particles, which reduced the thermal impact on the cBN particles. The cBN particles of the composite coatings were sharp and angular, which indicates that the raw cBN particles were well retained in the LC composite coatings. However, a reaction layer with a thickness of 2–5  $\mu\text{m}$  was formed on the bonding interface between the Ti6Al4V alloy matrix and cBN particles. The EDS results in the reaction layer indicated that Ti elements from the Ti6Al4V alloy and N elements from cBN could react to form a TiN reaction layer at the interface. Wang et al. also proved that the Ti elements of Co-based active filler metal produced a continuous reaction layer with a uniform thickness at the metal/cBN interface, when the brazing temperature was between 1473 and 1523 K [20].

According to the XRD results of the NicBN/Ti6Al4V composite coating, there were Ti solid solution, TiN, TiB<sub>x</sub>, and BN phases in the composite coating. This demonstrates that the decomposition of the cBN particles in the laser molten pool were converted into TiB<sub>x</sub> and TiN phases. Compared with the XPS results of the original cBN particles, the binding energy of B in the composite coating was 187.07 eV, indicating that part of the B from the cBN particle was converted to the TiB phase; the standard binding energy of N element in the BN compound was 398 eV. The binding energies of N in cBN particles of the composite coating were 397.13 and 398.8 eV, which indicates that part of nitrogen is prone to react to form TiN. Wang et al. and Gupta et al. reported that the formation of TiN and TiB intermetallic compounds took place between reinforcement and the matrix composition and also contributed to the creation of the metallurgical bonding between the particles of Ti6Al4V/cBN [16,20].

B and N atoms in the cBN and Ti atoms in the Ti6Al4V alloy matrix clustered at the interface. The atomic radius of B and N were 0.082 and 0.075 nm, respectively, whereas the diffusion coefficients of B and N in Ti were  $4.8 \times 10^{-7} \exp(-5600/T) \text{ cm}^2/\text{s}$  and  $4.5 \times 10^{-3} \exp(-6700/T) \text{ cm}^2/\text{s}$ , respectively. The atomic radius of N was lower than that of B, whereas the diffusion coefficient of N in Ti was higher when compared with B. The N atom in the cBN particle will first react with the Ti atom. The remaining B atom is prone to acquire Ti from TiN and the Ti6Al4V alloy matrix, as B would react with TiN or the B would directly react with Ti6Al4V at the interface near the cBN [16,20–22]. The reaction at the interface is



According to the results, the formation mechanism of the interfacial reaction layer of cBN particles in the composite coating is shown in Figure 12. The interfacial reaction of the cBN particles in the composite coating occurred in the laser molten pool. The active Ti atom from the Ti6Al4V alloy matrix easily acquired the N atom from the cBN particles, and then the Ti and N elements reacted to generate the TiN transition layer at the interface. Li et al. [23] also proved that BN particles reacted with

molten titanium to form TiN when the surface temperature was lower than the melting point of BN. The TiN reaction layer at the interface can act like a shield to effectively prevent cBN particles from further decomposing.

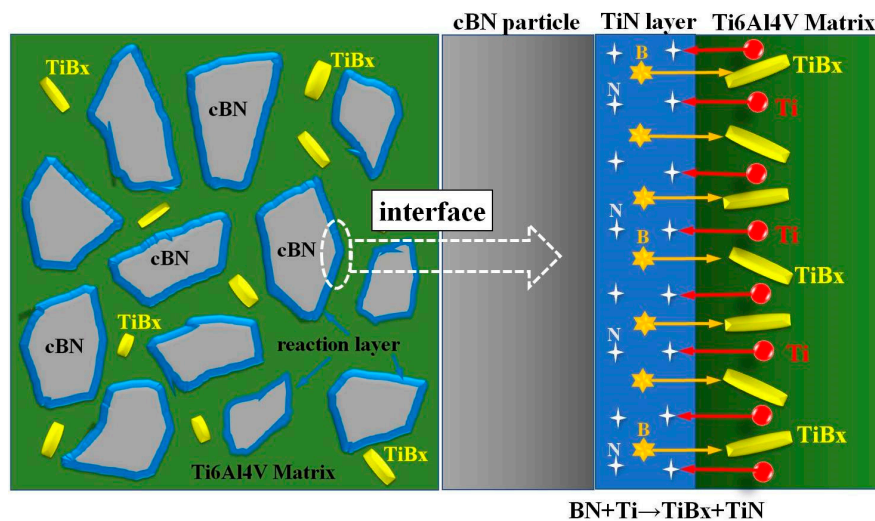


**Figure 12.** Reaction mechanism of the transition layer at the interface between the cBN particles and Ti6Al4V alloy matrix.

According to the wear results of the composite coatings, the friction coefficient of the Ni/cBN/Ti6Al4V composite coating was lower than that of the cBN/Ti6Al4V composite coating. The SEM images of both composite coatings demonstrated that the cBN particles in the cBN/Ti6Al4V composite coating were severely cracked and fell off under the rolling action of the  $\text{Si}_3\text{N}_4$  ball. On the contrary, the Ni coated cBN particle in the Ni/cBN/Ti6Al4V composite coating exhibited a better resistance to damage.

Kuang et al. also found that the fracture evolution from strong to weak bonding strength of abrasive cBN particles was from trans-granular to inter-granular for cBN abrasives [24]. The thermal conductivity (15.24 W/(m K)) of pure Ti is approximately one-third that of pure Fe. The friction heat accumulated in the composite coatings during the rotating sliding process helped to soften and oxidize the worn track. The cracked cBN debris under the action of rotating  $\text{Si}_3\text{N}_4$  ball consequently aggravated the abrasive wear between the composite coating and the ball as a third body. Thus, the wear mechanisms of the composite coating were primarily adhesive wear, oxidation wear, and abrasive wear. The above results demonstrated that the Ni plating on the surface of the cBN particles and the TiN reaction layer could effectively protect the cBN particles from the thermal defects and retain the raw properties of the cBN particles. This is beneficial for improving the wear resistance of the composite coatings.

## 5. Conclusions

The denser Ni/cBN/Ti6Al4V composite coating on the Ti6Al4V substrate was achieved in comparison with the cBN/Ti6Al4V composite coating using the LC process. The cBN particles retained the original shape in the composite coating. Thermal cracks were found on the surface of the cBN particles of the cBN/Ti6Al4V composite coating. The cBN particles in both composite coatings were coated with a 2–5  $\mu\text{m}$  reaction layer between the cBN particles and Ti6Al4V matrix. The XRD, EDS, and XPS results showed that the active Ti element from the Ti6Al4V alloy matrix and the N element from the surface of the cBN particles reacted to generate the TiN transition layer at the interface. The TiN transition layer effectively prevented the further decomposition of the cBN particles like a shield.

The Ni/cBN/Ti6Al4V composite coating presented better resistance to damage in comparison with the cBN/Ti6Al4V composite coating in the dry abrasive process, due to the Ni plating on the surface of

the cBN particles, which effectively reduced the cracking and fall off of cBN particles under the rolling action of the Si<sub>3</sub>N<sub>4</sub> ball. The wear mechanisms of the composite coating were primarily adhesive wear, oxidation wear, and abrasive wear. Ni plating on the surface of the cBN particles and the TiN reaction layer formed in the laser cladding process demonstrated a protective effect in preventing thermal defects and retaining the raw properties of the cBN particles. The discovery of the TiN reaction layer at the interface near the cBN particles in both the composite coatings can provide a new method to restrain the decomposition of cBN particles in the LC process.

**Author Contributions:** Conceptualization, L.Y.; data curation, S.F. and L.Y.; formal analysis, S.F. and L.Y.; investigation, S.F., L.Y., and P.W.; methodology, L.Y.; project administration, S.W. and Z.L.; resources, S.W. and Z.L.; software, S.F.; validation, S.F. and L.Y.; visualization, P.W. and S.W.; writing – original draft, S.F.; writing – review & editing, L.Y. All authors have read and agreed to the published version of the manuscript.

**Funding:** The authors would like to appreciate the financial supports from the National Natural Science Foundation of China (51701165), the Natural Science Foundation of Shaanxi Province (2018JM5005), Postdoctoral Science Foundation of China (2017M623334XB) and Shaanxi Province Postdoctoral Science Foundation (2018BSHQYXMZZ36).

**Conflicts of Interest:** The authors declare no conflict of interest.

## References

1. Zhang, X.S.; Chen, Y.J.; Hu, J.L. Recent advances in the development of aerospace materials. *Prog. Aerosp. Sci.* **2018**, *97*, 22–34. [[CrossRef](#)]
2. Xue, W.H.; Gao, S.Y.; Duan, D.L.; Zhang, J.P.; Liu, Y.; Li, S. Effects of blade material characteristics on the high-speed rubbing behavior between Al-hBN abradable seal coatings and blades. *Wear* **2018**, *410*, 25–33. [[CrossRef](#)]
3. Yao, J.H.; Yang, L.J.; Li, B. Beneficial effects of laser irradiation on the deposition process of diamond/Ni60 composite coating with cold spray. *Appl. Surf. Sci.* **2015**, *330*, 300–308. [[CrossRef](#)]
4. Luo, X.T.; Yao, M.L.; Ma, N.S.; Takahashi, M.; Li, C.J. Deposition behavior, microstructure and mechanical properties of an in-situ micro-forging assisted cold spray enabled additively manufactured Inconel 718 alloy. *Mater. Des.* **2018**, *155*, 384–395. [[CrossRef](#)]
5. Selivanov, K.S.; Smyslov, A.M.; Dyblenko, Y.M.; Semenova, I.P. Erosive wear behavior of Ti/Ti (V, Zr) N multilayered PVD coatings for Ti-6Al-4V alloy. *Wear* **2019**, *418*, 160–166. [[CrossRef](#)]
6. Zuo, Y.; Li, T.L.; Yu, P.H.; Zhao, Z.C.; Chen, X.Y.; Zhang, Y.; Chen, F. Effect of graphene oxide additive on tribocorrosion behavior of MAO coatings prepared on Ti6Al4V alloy. *Appl. Surf. Sci.* **2019**, *480*, 26–34. [[CrossRef](#)]
7. Zhou, H.H.; Liao, Z.W.; Fang, C.X.; Li, H.X.; Feng, B.; Song, X.; Cao, G.F.; Kuang, Y.F. Pulse electroplating of Ni-W-P coating and its anti-corrosion performance. *Trans. Nonferrous Met. Soc. China* **2018**, *28*, 88–95. [[CrossRef](#)]
8. Contin, A.; Vasconcelos, G.; Barquete, D.M.; Campos, R.A.; Trava-Airoldi, V.J.; Corat, E.J. Laser cladding of SiC multilayers for diamond deposition on steel substrates. *Diam. Relat. Mater.* **2016**, *65*, 105–114. [[CrossRef](#)]
9. Rajak, D.K.; Pagar, D.D.; Kumar, R.; Pruncu, C.I. Recent progress of reinforcement materials: A comprehensive overview of composite materials. *J. Mater. Res. Technol.* **2019**, *8*, 6354–6374. [[CrossRef](#)]
10. Ichida, Y. Mechanical properties and grinding performance of ultrafine-crystalline cBN abrasive grains. *Diam. Relat. Mater.* **2008**, *17*, 1791–1795. [[CrossRef](#)]
11. Liu, S.X.; Xiao, B.; Zhang, Z.Y.; Duan, D. Microstructural characterization of diamond/CBN grains steel braze joint interface using Cu–Sn–Ti active filler alloy. *Int. J. Refract. Met. Hard Mater.* **2016**, *54*, 54–59. [[CrossRef](#)]
12. Uhlmann, E.; Oyanedel Fuentes, J.A.; Keunecke, M. Machining of high performance workpiece materials with CBN coated cutting tools. *Thin Solid Films* **2009**, *518*, 1451–1454. [[CrossRef](#)]
13. Thepsonthi, T.; Özel, T. Experimental and finite element simulation based investigations on micro-milling Ti-6Al-4V titanium alloy: Effects of cBN coating on tool wear. *J. Mater. Process. Technol.* **2013**, *213*, 532–542. [[CrossRef](#)]
14. Luo, X.T.; Li, C.J. Tailoring the composite interface at lower temperature by the nanoscale interfacial active layer formed in cold sprayed cBN/NiCrAl nanocomposite. *Mater. Des.* **2018**, *140*, 387–399. [[CrossRef](#)]

15. Lu, X.L.; Liu, X.B.; Yu, P.C.; Zhai, Y.J.; Qiao, S.J.; Wang, M.D.; Wang, Y.G.; Chen, Y. Effects of heat treatment on microstructure and mechanical properties of Ni60/h-BN self-lubricating anti-wear composite coatings on 304 stainless steel by laser cladding. *Appl. Surf. Sci.* **2015**, *355*, 350–358. [[CrossRef](#)]
16. Gupta, A.; Hussain, M.; Misra, S.; Das, A.K.; Mandal, A. Processing and characterization of laser sintered hybrid B4C/cBN reinforced Ti-based metal matrix composite. *Opt. Lasers Eng.* **2018**, *105*, 159–172. [[CrossRef](#)]
17. Pacella, M.; Butler-Smith, P.W.; Axinte, D.A.; Fay, M.W. The allotropic transformation of polycrystalline cubic boron nitride structures resulting from the thermal effects of pulsed laser ablation. *Diam. Relat. Mater.* **2015**, *59*, 62–68. [[CrossRef](#)]
18. Yedave, S.N.; Malshe, A.P.; Brown, W.D.; Russell, W.C. Novel composite CBN-TiN coating: synthesis and performance analysis. *J. Manuf. Process.* **2003**, *5*, 154–162. [[CrossRef](#)]
19. Al-Hamdani, K.S.; Murray, J.W.; Hussain, T.; Clare, A.T. Controlling ceramic-reinforcement distribution in laser cladding of MMCs. *Surf. Coat. Technol.* **2020**, *381*, 125128. [[CrossRef](#)]
20. Wang, Y.; Duan, Z.Z.; Chen, G.; Jiang, Q.Y.; Dong, W.; Lei, K. Effects of brazing temperature on microstructure and properties of interface between cBN and Co-based active filler metals. *Vacuum* **2017**, *145*, 30–38. [[CrossRef](#)]
21. Senthil Selvan, J.; Subramanian, K.; Nath, A.K.; Kumar, H.; Ramachandra, C.; Ravindranathan, S.P. Laser boronising of Ti-6Al-4V as a result of laser alloying with pre-placed BN. *Mater. Sci. Eng. A.* **1999**, *260*, 178–187. [[CrossRef](#)]
22. Traxel, K.D.; Bandyopadhyay, A. Reactive-deposition-based additive manufacturing of Ti-Zr-BN composites. *Addit. Manuf.* **2018**, *24*, 353–363. [[CrossRef](#)]
23. Li, M.; Huang, J.; Zhu, Y.Y.; Li, Z.G. Effect of heat input on the microstructure of in-situ synthesized TiN-TiB/Ti based composite coating by laser cladding. *Surf. Coat. Technol.* **2012**, *206*, 4021–4026. [[CrossRef](#)]
24. Kuang, W.J.; Zhao, B.; Yang, C.Y.; Ding, W.F. Effects of h-BN particles on the microstructure and tribological property of self-lubrication CBN abrasive composites. *Ceram. Int.* **2020**, *46*, 2457–2464. [[CrossRef](#)]



© 2020 by the authors. Licensee MDPI, Basel, Switzerland. This article is an open access article distributed under the terms and conditions of the Creative Commons Attribution (CC BY) license (<http://creativecommons.org/licenses/by/4.0/>).